frontiers in Energy Research

ORIGINAL RESEARCH
published: 13 January 2021
doi: 10.3389/fenrg.2020.606023

Preparation of $Li_{2-3x}Al_xS$ for All-Solid-State Li-S Battery

Nguyen Huu Huy Phuc, Maeda Takaki, Muto Hiroyuki and Matsuda Atsunori**

Department of Electrical and Electronic Information Engineering, Toyohashi University of Technology, Toyohashi, Japan

$Li_{2-3x}Al_xS$ ($0 \leq x \leq 0.1667$) was prepared via the planetary ball-milling method. Diffuse reflection UV-Vis measurements revealed that the band gap and electronic structure of Li_2S changed with the formation of defective $Li_{2-3x}Al_xS$. Compared with $x = 0$, the ionic conductivity for the sample with $x = 0.1334$ improved by ~3 orders of magnitude. The lithium movement activation energy and pre-exponential factor A were found to be dependent on the x value. Compared with Li_2S, a ~10-fold improvement in the electronic conductivity was realized with the addition of Al_2S_3. Additionally, the all-solid-state Li-S battery cell performance also displayed an enhancement in both the initial capacity and stability for sample $x = 0.1667$ compared with $x = 0$. This study highlighted the importance of the intrinsic electronic conductivity of the active materials (but not the electrode) on the performance of the all-solid-state Li-S battery.

Keywords: lithium sulfur battery, Li-S battery, Li_2S conductivity, all-solid-state, mutivalence cation

OPEN ACCESS

Edited by:
Candace K. Chan,
Arizona State University, United States

Reviewed by:
Shichun Mu,
Wuhan University of Technology, China
Yong Yang,
Xiamen University, China

****Correspondence:***
Nguyen Huu Huy Phuc
nguyen.huu.huy.phuc.hr@tut.jp
Matsuda Atsunori
matsuda@ee.tut.ac.jp

Specialty section:
This article was submitted to Electrochemical Energy Conversion and Storage, a section of the journal Frontiers in Energy Research

Received: *14 September 2020*
Accepted: *04 December 2020*
Published: *13 January 2021*

Citation:
Phuc NHH, Takaki M, Hiroyuki M and Atsunori M (2021) Preparation of $Li_{2-3x}Al_xS$ for All-Solid-State Li-S Battery. Front. Energy Res. 8:606023. doi: 10.3389/fenrg.2020.606023

INTRODUCTION

Lithium-sulfur (Li-S) batteries have attracted significant attention because of their high theoretical energy density (Yang et al., 2013). Research on Li-S batteries has progressed in various directions, including towards understanding the charging-discharging mechanism, irreversible capacity, and cathode composite structure. Many types of electrolytes have been employed in Li-S batteries to date, such as liquid electrolytes, liquid ionic electrolytes, sulfide solid electrolytes, oxide-based solid electrolytes, and polymer electrolytes. The use of either conventional liquid electrolytes or liquid ionic electrolytes has issues related with the formation and dissolution of polysulfides; this results in the loss of active material in the cathode and, thus, a reduced cell capacity or the migration and deposition of polysulfides on the anode, which terminates the cycling process (Li G. et al., 2018). The suppression of polysulfide dissolution and migration could be enabled via various methods, including absorption on large surface area materials, design of the cathode structure, the use of separators, and replacement of the liquid electrolyte with a solid electrolyte (Hayashi et al., 2003; Hayashi et al., 2008; Nishio et al., 2009; Pan et al., 2017; He et al., 2018; Yun et al., 2018).

In general, there are three types of Li-S batteries that employ either sulfur, lithium sulfide, or metal sulfide as the active material (Yao et al., 2016; Li M. et al., 2018). The use of either sulfur or a metal sulfide as the active material provides the benefit of facile cathode composite preparation, due to their stability in the ambient atmosphere; the anode in this case must contain lithium, such as lithium metal or a lithium alloy. However, the use of Li_2S limits the available composite preparation methods because it is unstable in an ambient atmosphere and reacts with moisture to release hydrogen sulfide. Hence, the use of common anode materials, such as graphite and silicon, is desired because they are safer than lithium.

Sulfide solid electrolytes are materials based on Li_2S-P_2S_5 and have high ionic conductivities and unique mechanical properties, so have attracted significant research attention in the domain of solid-

state ionic materials (Lau et al., 2018). Li_2S-P_2S_5 glass-ceramic solid electrolytes generally exhibit decent ionic conductivities of ~10^{-4}–10^{-2} Scm^{-1} at room temperature (Tatsumisago and Hayashi, 2012; Seino et al., 2014). The addition of a lithium halide, generally LiI, could further increase the ionic conductivity of the Li_3PS_4 solid electrolyte from 10^{-4} to 10^{-3} Scm^{-1} at room temperature (Han et al., 2018; Feng et al., 2019; Spannenberger et al., 2019). $Li_{10}GeP_2S_{12}$ and related materials have been reported to have ionic conductivities of up to 10^{-2} Scm^{-1} with an Li ion transference number of nearly 1 (Kamaya et al., 2011; Kato et al., 2016). Argyrodite-type solid electrolytes, which are derived from Li_7PS_6, have also been able to realize ionic conductivities of 10^{-2} Scm^{-1} at room temperature (Adeli et al., 2019).

Li_2S is partially an electric insulator and has extremely poor ionic conductivity at room temperature. Some controversy exists regarding the ionic conductivity of Li_2S. Lin et al. previously reported a value lower than 10^{-13} Scm^{-1} at room temperature (value extrapolated from their report) (Lin et al., 2013). Subsequently, Hakari et al. observed an ionic conductivity as high as 10^{-8} Scm^{-1} at room temperature for Li_2S pretreated via planetary ball milling (Hakari et al., 2017). Lorger et al. published a systematic study on the ionic conductivity of Li_2S and concluded that single-crystal Li_2S had a conductivity of ~10^{-8} Scm^{-1} at room temperature (Lorger et al., 2018). Because of its low intrinsic conductivity, Li_2S is usually been blended with both electronic and ionic conductors to prepare electrode composites for application in Li-S batteries.

All-solid-state (ASS) Li-S batteries employing sulfidic solid electrolytes (SE) and Li_2S have advantages in cathode composite preparation because the sulfidic SE is usually synthesized from Li_2S and P_2S_5. Nano Li_2S coated with Li_3PS_4 was prepared via a reaction between nano Li_2S and P_2S_5 with a molar ratio of 9:1 in tetrahydrofuran (THF) (Lin et al., 2013). In the same manner, Li_2S@Li_3PS_4 was prepared via either planetary ball milling or liquid-phase synthesis for application in the ASS Li-S battery (Jiang et al., 2019; Jiang et al., 2020). Nano composites of Li_2S and carbonaceous materials were also generated using various methods for battery application. Typically, Li_2S was dissolved in ethanol and the electronic conductor was then immersed into the solution; this was followed by solvent evaporation and subsequent heat treatment (Eom et al., 2017). Li_2S embedded in a carbon matrix was also generated *in-situ* via the reaction between CS_2 and lithium at a high temperature in an auto clave (Han et al., 2016).

A solid solution of Li_2S-LiX (X = Cl, Br, I) improved the low intrinsic ionic conductivity of Li_2S, but the effect on battery performance originated from an increase in redox centers due to I^- incorporation (Hakari et al., 2017). Recently, Nguyen et al. showed that the conductivity of Li_3PS_4 was drastically improved at temperatures higher than room temperature via doping with a multivalence cation (Ca^{2+}, Mg^{2+}) (Phuc et al., 2020a). In this study, $Li_{2-3x}Al_xS$ samples were prepared via planetary ball milling for application in an ASS Li-S battery. Argyrodite-type $Li_{5.5}PS_{4.5}Cl_{1.5}$ was synthesized and employed as the solid electrolyte in the battery performance test. The addition of Al_2S_3 improved not only the ionic conductivity of Li_2S but also Li_2S utilization in the ASS Li-S battery.

EXPERIMENTAL

Li_2S (99.9%, Mitsuwa), P_2S_5 (99%, Merck), LiCl (99.99%, Wako Fujifilm), and Al_2S_3 (99.9%, Kojundo Laboratory) were used as received.

$Li_{2-3x}Al_xS$ ($0 \leq x \leq 0.1667$) was prepared via planetary ball milling. Li_2S and Al_2S_3 were mixed for 10 min using an agate mortar, and then put into a 45-ml zirconia pot with zirconia balls (10 mm, 15 balls). The pots were rotated at 500 rpm for 12 h using a Pulverisette 7 (Fritsch). The obtained samples were recovered and used without any further heat treatment.

Then, 1 g of Li_2S, P_2S_5, and LiCl with the molar ratio required to form $Li_{5.5}PS_{4.5}Cl_{1.5}$ was mixed in an agate mortar. The obtained mixture was then ball milled at 600 rpm for 24 h. The as-obtained sample was further heat treated at 440°C for 2 h to obtain the $Li_{5.5}PS_{4.5}Cl_{1.5}$ argyrodite-type SE with an ionic conductivity of 2.8×10^{-4} Scm^{-1} at room temperature.

A composite cathode composed of $Li_{2-3x}Al_xS$, $Li_{5.5}PS_{4.5}Cl_{1.5}$, and Ketjen Black (KB) with a weight ratio of 50:40:10 was prepared via planetary ball milling. Zirconia balls (160 ball, 4 mm) and a 300-mg of mixture of (100–x) Li_2S–xAl_2S_3 and $Li_{5.5}PS_{4.5}Cl_{1.5}$, KB were placed into a 45-ml zirconia pot, and the two pots were then rotated at 510 rpm for 10 h. Composites containing $Li_{2-3x}Al_xS$ and KB (without $Li_{5.5}PS_{4.5}Cl_{1.5}$) were also prepared and their cycling performance in an ASS Li-S battery was investigated.

The structure of the prepared $Li_{2-3x}Al_xS$ powders was characterized via X-ray diffraction (XRD; Ultima IV, Rigaku), Raman spectroscopy (NRS-3100, Jasco), and diffuse reflection UV-Vis spectroscopy (V-670, Jasco). For analysis, the samples were sealed in special holders in an Ar-filled glove box to avoid exposure to humidity.

The temperature dependence of the ionic conductivity of the prepared samples was investigated using a previously reported procedure (Phuc et al., 2017). The conductivity at room temperature was measured via the direct current polarization method. Prior to the measurements, the samples were pressed into pellets of ~10 mm in diameter at a pressure of 550 MPa (at room temperature). The pellets were then placed in a PEEK holder with two stainless steel rods as blocking electrodes. Voltages of 0.2, 0.5, and 1.0 V (DC) were then applied to the prepared cells for 60 min and the current was measured. The experiments were carried out using potentiostat SI 1287 (Solatron). ASS Li-S cells were fabricated with a structure resembling one reported elsewhere (Phuc et al., 2020c). All the experiments were conducted in an Ar-filled glove box (water <0.1 ppm) or an airtight sample holder to avoid the direct exposure of the samples to ambient humidity.

RESULTS AND DISCUSSION

Figure 1 shows the structural characteristics of $Li_{2-3x}Al_xS$ ($0 \leq x \leq 0.1667$) investigated via powder XRD, Raman spectroscopy, and diffuse reflection UV-Vis spectroscopy. The XRD patterns (**Figure 1A**) displayed only the peaks of Li_2S without any features of the Al_2S_3 structure. This indicated that either Al_2S_3

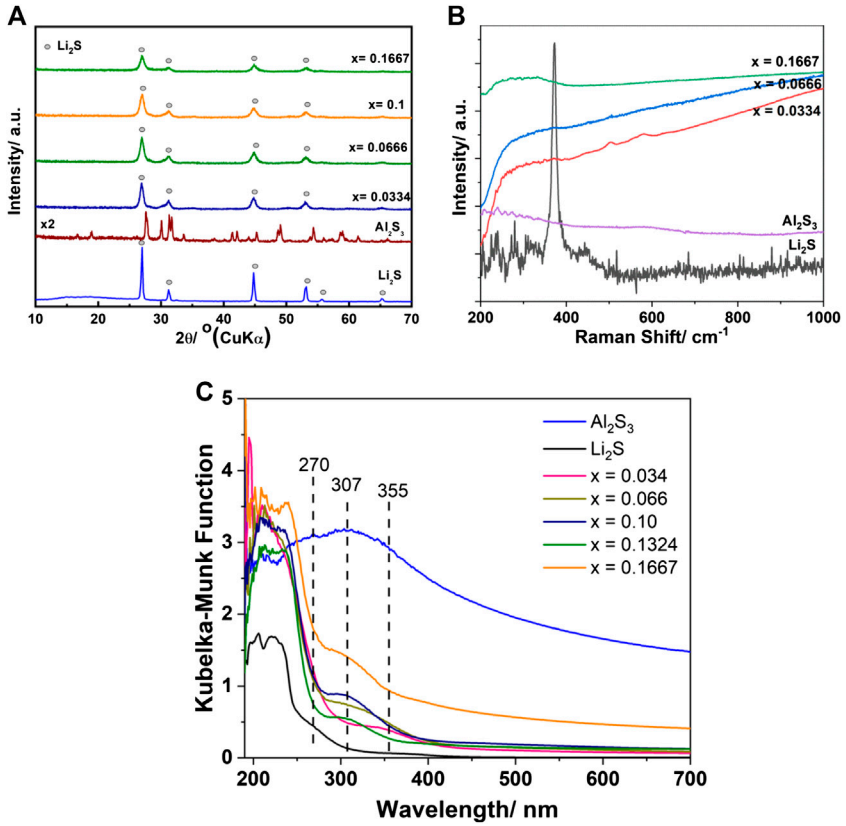

FIGURE 1 | Structure characterization of $Li_{2-3x}Al_xS$ ($0 \le x \le 0.1667$) samples. **(A)** XRD patterns; **(B)** Raman spectra; and **(C)** UV-Vis spectra of $Li_{2-3x}Al_xS$ ($0 \le x \le 0.1667$) samples.

formed a solid solution with Li_2S or that Al_2S_3 was present in the amorphous form together with the Li_2S crystal. The Raman spectrum of Li_2S showed one sharp peak located at 372 cm^{-1} (**Figure 1B**). Al_2S_3 exhibited many small peaks in the range of 200–300 cm^{-1} with one peak at 240 cm^{-1} that had a slightly higher intensity than the others. The Al_2S_3 spectrum resembled previously reported results for α-Al_2S_3 (Haeuseler et al., 1981). The sample $Li_{2-3x}Al_xS$ had nearly no special features in the measured range of 200–1,000 cm^{-1} except for a shoulder between 200 and 400 cm^{-1}. The peak for Li_2S was absent in the spectra and the peaks for Al_2S_3 were extremely weak, and hence, hard to detect. It was observed that the Raman peaks of graphene and the carbon nanotube were drastically altered or even disappeared because of the disorder in the local structure, which resulted from defect introduction (Eckmann et al., 2013). For the UV-Vis absorption measurements, Li_2S exhibited one small shoulder centered at 270 nm and a large shoulder in the range of 250–190 nm (**Figure 1C**). Al_2S_3 showed a large absorption shoulder ranging from ~400 to 190 nm. The addition of a small amount of Al_2S_3 into Li_2S (x = 0.034) led to the formation of $Li_{1.9}Al_{0.034}S$ and resulted in a drastic change in the electronic structure of the material when compared with its constituent raw materials, Li_2S and Al_2S_3. The adsorption shoulder of Li_2S centered at 270 nm and the large adsorption shoulder of Al_2S_3 disappeared along with the appearance of a new adsorption band centered at 355 nm. This special absorption band was also observed in other samples. The absorption feature of Al_2S_3 was detected in the sample with $x \ge 0.066$, but the shoulder of Li_2S located at 270 nm completely disappeared. It should be noted that the milled Li_2S showed no absorption in the visible range (400–800 nm), but the absorption shoulder of the $Li_{2-3x}Al_xS$ ($0 \le x \le 0.1667$) samples could be tailored from the UV to the visible spectral range; in particular, the sample x = 0.1667 exhibited a drastic adsorption enhancement in the visible range compared with Li_2S and the other samples. The diffuse reflection UV-Vis measurements revealed that the band gap and electronic structure of Li_2S changed with the formation of $Li_{2-3x}Al_xS$, even though the XRD measurements showed no change in the Li_2S crystal structure. Thus, it can be concluded that defect-rich $Li_{2-3x}Al_xS$ was formed by doping of Al_2S_3 to Li_2S via the planetary ball-milling method.

Figure 2 shows the temperature dependence of the ionic conductivity, the ionic conductivity at 50°C, the activation energy, the pre-exponential factor A, electronic conductivity, and their I-V correlation as a function of x in the $Li_{2-3x}Al_xS$ ($0 \le x \le 0.1667$) samples. The ionic conductivity of bare Li_2S (after planetary ball milling) was ~10^{-10} Scm^{-1} at room temperature. This value was extrapolated from the temperature dependence of the ionic conductivity because the resistivity was too large to measure. The value of 10^{-8} Scm^{-1} displayed in **Figure 2B** was

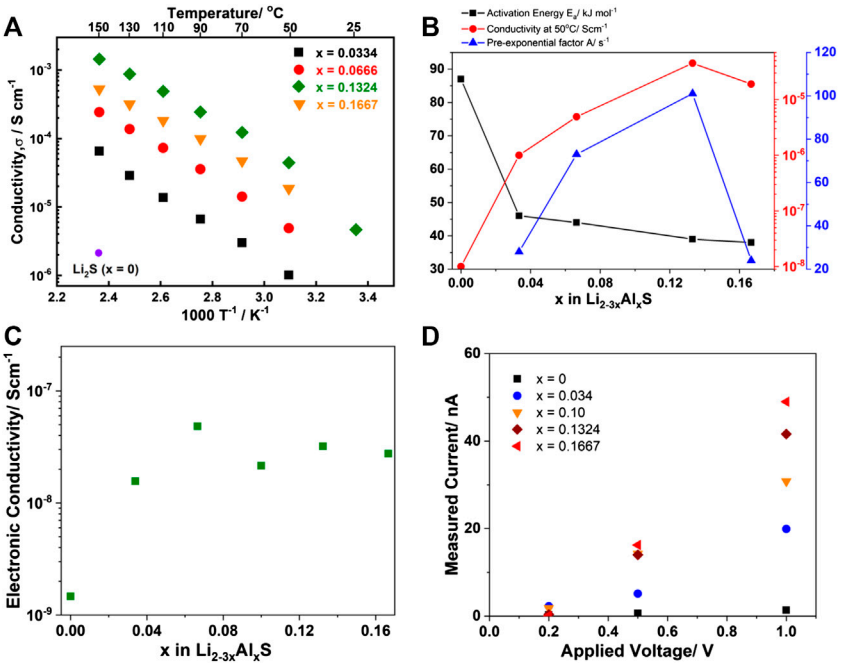

FIGURE 2 | Conduction properties of the $Li_{2-3x}Al_xS$ ($0 \le x \le 0.1667$) samples. **(A)** Temperature dependence of ionic conductivity; **(B)** Activation energy (closed square), ionic conductivity at 50°C (closed circle), and pre-exponential factor A (closed triangle) as a function of *x*. Conductivity and activation energy of sample $x = 0$ in **A,B** were adapted from references (Hakari et al., 2017; Lorger et al., 2018); **(C)** Electronic conductivity as a function of *x*; and **(D)** I–V correlation of the $Li_{2-3x}Al_xS$ ($0 \le x \le 0.1667$) samples.

obtained from references (Hakari et al., 2017; Lorger et al., 2018). Compared with $x = 0$, the ionic conductivity drastically improved with the addition of Al_2S_3. For example, the conductivity at 150 °C increased by three orders of magnitude for sample $x = 0.1334$. The activation energy of bare Li_2S was ~86 kJ mol^{-1} and the addition of a small amount of Al_2S_3 into Li_2S led to a decrease in the activation energy to 44 kJ mol^{-1} ($x = 0.0334$). Further addition of Al_2S_3 only resulted in a slight improvement to 38 kJ mol^{-1} ($x = 0.1667$). The ionic conductivity at 50°C had the opposite trend as the activation energy. The addition of Al^{3+} into Li_2S enhanced the ionic conductivity and reached a peak at $x = 0.1334$. Further Al^{3+} addition resulted in a slight decrease in the ionic conductivity. The pre-exponential factor A was also calculated, as illustrated in **Figure 2B**. The value had the same trend as the ionic conductivity and reached a maximum value at $x = 0.1334$, and then drastically decreased with the further increase of *x*. These results suggest that the addition of Al^{3+} into Li_2S led to an improvement of both the ionic conductivity and the activation energy because of defect formation. The results obtained in this study also differed from the reported observations when Na_3PS_4 or Li_3PS_4 were doped with multi-valence cations, which resulted in both the ionic conductivity and activation energy increasing with the addition of Ca^{2+} or Mg^{2+} (Moon et al., 2018; Phuc et al., 2020a). The electronic conductivity (electron conductivit¯y) of $Li_{2-3x}Al_xS$ ($0 \le x \le 0.1667$) was measured using blocking electrodes, as illustrated in **Figure 2C**. The bare Li_2S exhibited an electronic conductivity of ~1.5×10^{-9} Scm^{-1} at room temperature. $Li_{2-3x}Al_xS$ ($0 < x \le 0.1667$) showed an improvement in the electronic conductivity that was 10-fold higher than Li_2S, and there was nearly no observable difference between the measured doped samples. The results of the I–V correlation measurements using blocking electrodes are shown in **Figure 2D**. The result confirmed that Li_2S was nearly insulating towards electrons at applied voltages up to 1 V. The current in the doped samples clearly exhibited a dependence on the applied voltage. The dependence of the electronic current on *x* at every applied voltage was investigated; sample $x = 0.1667$ exhibited a higher current than $x = 0.1324$. These results differed from those obtained for the ionic conductivity. In a reported theoretical study, density function theory (DFT) was employed to investigate the effect of transition metal (Fe, Cu, Co, Ni) doping on the Li redox properties and electrode potential of Li_2S (Luo et al., 2012). It was found that Fe doping could lower the band gap of Li_2S because Fe-S (Fe 3d and S 3p orbitals) gap state appeared between the S 3p valence band and the empty Li 2s states. Hence, the electronics structure of Fe doped Li_2S was altered from insulating to the conducting regimen. Therefore, improvement in the electronic conductivity of Al_2S_3-doped Li_2S was expected to originate from the electronic structure of the Al-S bonding, which filled the large gap between Li 2s and S 3d in intrinsic Li_2S. The electronic conductivity of $Li_{2-3x}Al_xS$ ($0 \le x \le 0.1667$) was independent of the Al content, but the polarization current values varied linearly with the applied voltage and Al content (**Figure 2D**). These results confirmed that the overlap of the Al-S and Li-S gap states could accommodate electron movement during Li insertion/extraction.

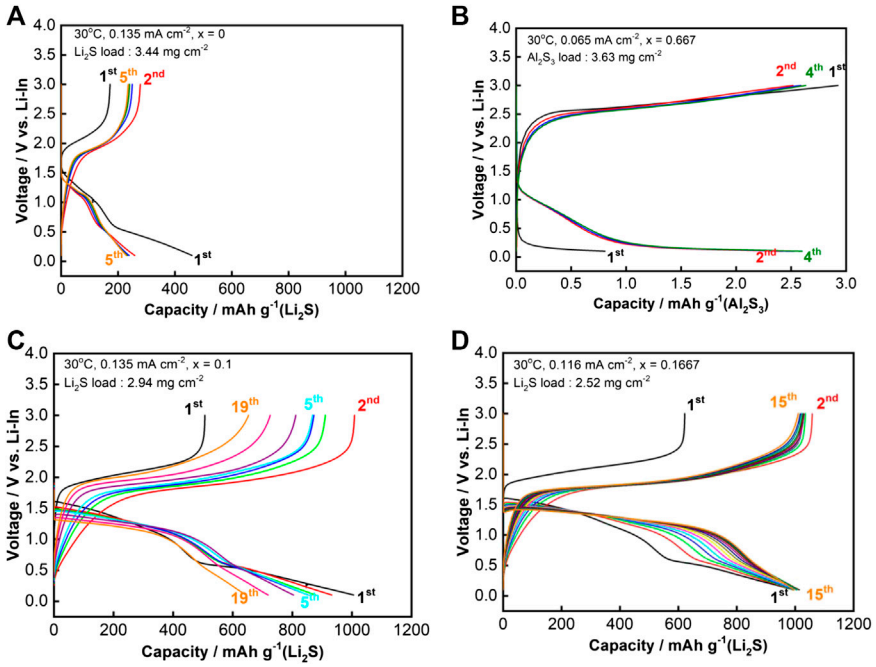

FIGURE 3 | Charge-discharge curves of the all-solid-state cells employing $Li_{2-3x}Al_xS$ ($0 \le x \le 0.1667$) cycled at room temperature. **(A)** $x = 0$ (Li_2S); **(B)** $x = 0.667$ (Al_2S_3); **(C)** $x = 0.1$; and **(D)** $x = 0.1667$.

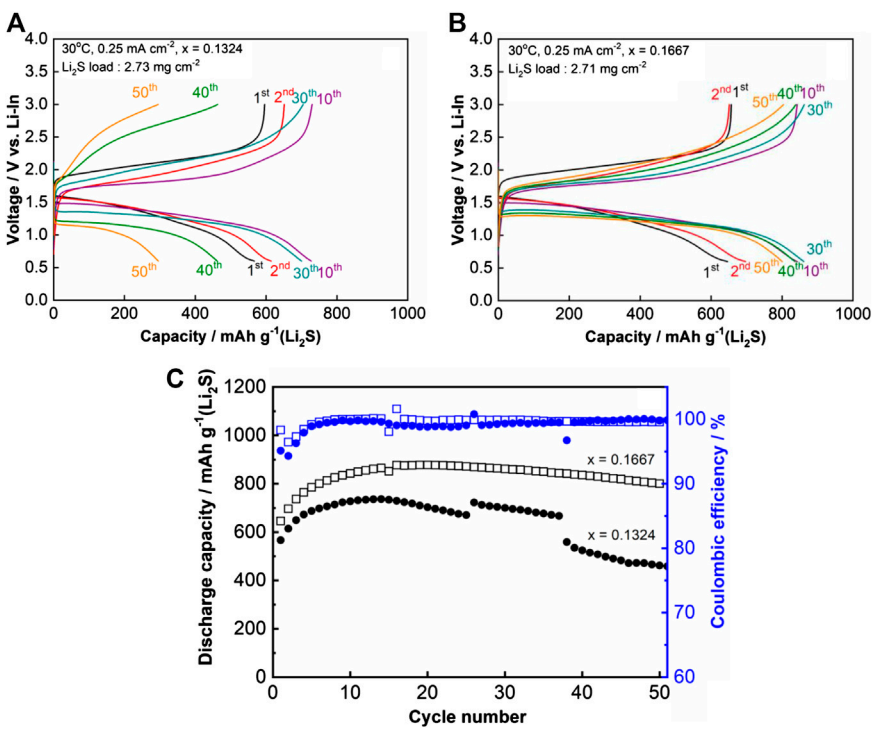

FIGURE 4 | Charge-discharge curves and cycling performance of the prepared all-solid-state cell. **(A)** charge-discharge curves of $x = 0.1324$; **(B)** $x = 0.1667$; and **(C)** cycling performance of $x = 0.1324$ and 0.1667 over 50 cycles at 30°C.

The charge-discharge curves of the ASA cells employing composite cathodes containing $Li_{2-3x}Al_xS$ are shown in **Figures 3A–D**. The cut off voltage was 3.0–0.1 V vs. Li-In and the prepared $Li_{5.5}PS_{4.5}Cl_{1.5}$ pellet served as a separator. The capacity of the sample with $x = 0$ (Li_2S) was demonstrated to be ~200 mAh g^{-1}_{Li2S} (**Figure 3A**). The cell containing only Al_2S_3 showed nearly no reversible reaction between Al_2S_3 and Li^+ and e^- (**Figure 3B**). A first charge capacity of 450 and discharge capacity of 1,000 mAh g^{-1}_{Li2S} were obtained with sample $x = 0.1$ (**Figure 3C**). Sample $x = 0.1667$ delivered capacities of 600 and 1,000 mAh g^{-1}_{Li2S} in the first charge-discharge cycle (**Figure 3D**). The discharge capacity of sample $x = 0.1667$ was maintained at ~1,000 mAh g^{-1}_{Li2S} over 15 cycles while the capacity of $x = 0.1$ rapidly decreased from 1,000 to 600 mAh g^{-1}_{Li2S} over 19 cycles. The addition of MgS into Li_2S also resulted in improvement of not only the ionic conductivity but also the all-solid-state cell capacity and cycling performance, as reported elsewhere (Phuc et al., 2020b). Discharge curves for the two samples displayed two distinct plateaus at ~1.5 and 0.5 V vs. Li-In. ASS Li-S batteries employing Li_2S as the active material had only one plateau in the discharge curve, hence the appearance of the second plateau at 0.5 V vs. Li-In (1.1 V vs. Li/Li^+) should originate from Al_2S_3 and the solid electrolyte (Nagao et al., 2015; Hakari et al., 2017; Tan et al., 2019). ASS Li-S batteries that employ a metal sulfide as the active material, e.g., CuS and NiS, exhibited two distinct plateaus in the discharge curves (Hayashi et al., 2003; Hayashi et al., 2008). The capacity of the second plateau in the reported batteries was stable during cell cycling, which indicated a reversible reaction between the metal sulfides and Li^+-e^-. Argyrodite-type solid electrolytes were also reported to be reduced in this voltage region, which was a reversible reaction (Tan et al., 2019). Therefore, the large capacity of ~500 mAh g^{-1} observed in the first discharge could be attributed to the reaction of both Al_2S_3 and the solid electrolyte. However, the second plateau observed in this study gradually disappeared when the cells were cycled. Thus, the differences in the discharge and charge capacity should originate from a reduction of Al_2S_3 in the electrode to form Li_2S and argyrodite to form Li_3PS_4, LiCl, Li_2S, and Li_3P. The stabilization of the electrode at $x = 0.1667$ was considered to be related to the formation of an unknown intermediate generated from Al_2S_3; this is because the capacity of the second plateau gradually reduced after the first cycle.

To investigate the effect of Al^{3+} doping on the cell performance without the contribution of a reaction at 0.5 V vs. Li-In, two cells composed of samples with $x = 0.1324$ and 0.1667 were cycled within a cut off voltage range of 3.0–0.6 V vs. Li-In. The results are shown in **Figures 4A–C**. Both cells exhibited a first charge-discharge capacity of ~600 mAh g^{-1}_{Li2S} (**Figures 4A,B**). These capacities differed from those observed when the cut off voltage was between 3.0 and 0.1 V. The discharge curves in this experiment also consisted of only one plateau. These results proved that the reduction reaction of Al_2S_3 was effectively suppressed by increasing the cut off voltage. The capacity of sample $x = 0.1324$ slightly increased from 600 to 700 mAh g^{-1}_{Li2S} in the first 10 cycles, and then reduced to ~400 mAh g^{-1}_{Li2S} after 50 cycles. In contrast, the cell with $x = 0.1667$ had its capacity increase from 600 mAh g^{-1}_{Li2S} to more than 800 mAh g^{-1}_{Li2S} in the first 10 cycles. Then, the capacity remained nearly stable and was maintained at a value of ~800 mAh g^{-1}_{Li2S} after 50 cycles (**Figure 4C**). These cyclic performances suggest that the higher ionic conductivity of $x = 0.1324$ compared with $x = 0.1667$ had a limited contribution to the cycling performance of the ASS cells. In addition, the electronic conductivity and polarizability on voltage application seemed to be the main reasons for the superior performance of $x = 0.1667$ compared with those of $x = 0$ and 0.1324.

CONCLUSION

Al_2S_3 was successfully incorporated into Li_2S to form a solid solution of $Li_{2-3x}Al_xS$ ($0 \le x \le 0.1667$) via planetary ball milling. It was found that the addition of Al^{3+} resulted in the formation of defects in the Li_2S structure, and thus improved the electronic conductivity, ionic conductivity, and activation energy. ASS Li-S cells employing $Li_{2-3x}Al_xS$ ($0 < x \le 0.1667$) had a higher capacity than those employing bare Li_2S. The addition of Al^{3+} ($x = 0.1667$) contributed to not only improving the initial capacity but also capacity retention because of a reduction in the activation energy for the sulfur, lithium ion, and electron combination reaction. The results from this study highlighted the importance of the intrinsic electronic conductivity of the active materials (but not the electrode) on the performance of all-solid-state Li-S batteries.

DATA AVAILABILITY STATEMENT

The original contributions presented in the study are included in the article/Supplementary Material, further inquiries can be directed to the corresponding authors.

AUTHOR CONTRIBUTIONS

MA and MH: supervision of this project, funding acquisition, manuscript revision. NP: experimental design, supervision, manuscript preparation. TM: data acquisition.

FUNDING

This study was supported by the Advanced Low Carbon Technology Specially Promoted Research for Innovative Next Generation Batteries program of the Japan Science and Technology Agency (JST-ALCA-SPRING, Grant No. JPMJAL1301).

ACKNOWLEDGMENTS

We thank Arun Paraecattil, PhD, from Edanz Group (https://en-author-services.edanzgroup.com/ac) for editing a draft of this manuscript.

REFERENCES

Adeli, P., Bazak, J. D., Park, K. H., Kochetkov, I., Huq, A., Goward, G. R., et al. (2019). Boosting solid-state diffusivity and conductivity in lithium superionic argyrodites by halide substitution. *Angew Chem. Int. Ed. Engl.* 58, 8681–8686. doi:10.1002/anie.201814222

Eckmann, A., Felten, A., Verzhbitskiy, I., Davey, R., and Casiraghi, C. (2013). Raman study on defective graphene: effect of the excitation energy, type, and amount of defects. *Phys. Rev. B* 88. doi:10.1103/PhysRevB.88.035426

Eom, M., Son, S., Park, C., Noh, S., Nichols, W. T., and Shin, D. (2017). High performance all-solid-state lithium-sulfur battery using a Li2S-VGCF nanocomposite. *Electrochim. Acta* 230, 279–284. doi:10.1016/j.electacta.2017.01.155

Feng, X., Chien, P.-H., Patel, S., Zheng, J., Immediato-Scuotto, M., Xin, Y., et al. (2019). Synthesis and characterizations of highly conductive and stable electrolyte $Li_{10}P_3S_{12}I$. *Energy Storage Mater.* 22, 397–401. doi:10.1016/j.ensm.2019.07.047

Haeuseler, H., Cansiz, A., and Lutz, H. D. (1981). Zur Kenntnis des Aluminiumsulfids: a-Al_2S_3 und Al_2S_3(tetr.). *Z. Naturforsch. B Chem. Sci.* 36, 532–534. doi:10.1515/znb-1981-0502

Hakari, T., Hayashi, A., and Tatsumisago, M. (2017). Li 2 S-based solid solutions as positive electrodes with full utilization and superlong cycle life in all-solid-state Li/S batteries. *Adv. Sustainable Syst.* 2017, 1700017. doi:10.1002/adsu.201700017

Han, F., Yue, J., Fan, X., Gao, T., Luo, C., Ma, Z., et al. (2016). High-performance all-solid-state lithium-sulfur battery enabled by a mixed-conductive Li2S nanocomposite. *Nano Lett.* 16, 4521–4527. doi:10.1021/acs.nanolett.6b01754

Han, F., Yue, J., Zhu, X., and Wang, C. (2018). Suppressing Li dendrite formation in Li_2S-P_2S_5 solid electrolyte by LiI incorporation. *Adv. Energy Mater.* 8, 1703644. doi:10.1002/aenm.201703644

Hayashi, A., Nishio, Y., Kitaura, H., and Tatsumisago, M. (2008). Novel technique to form electrode–electrolyte nanointerface in all-solid-state rechargeable lithium batteries. *Electrochem. Commun.* 10, 1860–1863. doi:10.1016/j.elecom.2008.09.026

Hayashi, A., Ohtomo, T., Mizuno, F., Tadanaga, K., and Tatsumisago, M. (2003). All-solid-state Li S batteries with highly conductive glass–ceramic electrolytes. *Electrochem. Commun.* 5, 701–705. doi:10.1016/S1388-2481(03)00167-X

He, Y., Qiao, Y., and Zhou, H. (2018). Recent advances in functional modification of separators in lithium-sulfur batteries. *Dalton Trans.* 47, 6881–6887. doi:10.1039/c7dt04717g

Jiang, H., Han, Y., Wang, H., Guo, Q., Zhu, Y., Xie, W., et al. (2019). In situ generated Li_2S-LPS composite for all-solid-state lithium-sulfur battery. *Ionics* 26, 2335–2342. doi:10.1007/s11581-019-03287-9

Jiang, H., Han, Y., Wang, H., Zhu, Y., Guo, Q., Jiang, H., et al. (2020). Li2S-Li3PS4 (LPS) composite synthesized by liquid-phase shaking for all-solid-state lithium-sulfur batteries with high performance. *Energy Technol.* 8. doi:10.1002/ente.202000023

Kamaya, N., Homma, K., Yamakawa, Y., Hirayama, M., Kanno, R., Yonemura, M., et al. (2011). A lithium superionic conductor. *Nat. Mater* 10, 682–686. doi:10.1038/nmat3066

Kato, Y., Hori, S., Saito, T., Suzuki, K., Hirayama, M., Mitsui, A., et al. (2016). High-power all-solid-state batteries using sulfide superionic conductors. *Nat. Energy* 1, 16030. doi:10.1038/nenergy.2016.30

Lau, J., DeBlock, R. H., Butts, D. M., Ashby, D. S., Choi, C. S., and Dunn, B. S. (2018). Sulfide solid electrolytes for lithium battery applications. *Adv. Energy Mater.* 8, 1800933. doi:10.1002/aenm.201800933

Li, G., Wang, S., Zhang, Y., Li, M., Chen, Z., and Lu, J. (2018). Revisiting the role of polysulfides in lithium-sulfur batteries. *Adv. Mater.* 30, e1705590. doi:10.1002/adma.201705590

Li, M., Chen, Z., Wu, T., and Lu, J. (2018). Li2 S- or S-based lithium-ion batteries. *Adv. Mater.* 30, e1801190. doi:10.1002/adma.201801190

Lin, Z., Liu, Z., Dudney, N. J., and Liang, C. (2013). Lithium superionic sulfide cathode for all-solid lithium-sulfur batteries. *ACS Nano.* 7, 2829–2833. doi:10.1021/nn400391h

Lorger, S., Usiskin, R. E., and Maier, J. (2018). Transport and charge carrier chemistry in lithium sulfide. *Adv. Funct. Mater.* 29. doi:10.1002/adfm.201807688

Luo, G., Zhao, J., and Wang, B. (2012). First-principles study of transition metal doped Li2S as cathode materials in lithium batteries. *J. Renew. Sustain. Energy* 4, 063128. doi:10.1063/1.4768814

Moon, C. K., Lee, H.-J., Park, K. H., Kwak, H., Heo, J. W., Choi, K., et al. (2018). Vacancy-driven Na+ superionic conduction in new Ca-doped Na3PS4 for all-solid-state Na-ion batteries. *ACS Energy Lett.* 3, 2504–2512. doi:10.1021/acsenergylett.8b01479

Nagao, M., Hayashi, A., Tatsumisago, M., Ichinose, T., Ozaki, T., Togawa, Y., et al. (2015). Li2S nanocomposites underlying high-capacity and cycling stability in all-solid-state lithium–sulfur batteries. *J. Power Sources* 274, 471–476. doi:10.1016/j.jpowsour.2014.10.043

Nishio, Y., Kitaura, H., Hayashi, A., and Tatsumisago, M. (2009). All-solid-state lithium secondary batteries using nanocomposites of NiS electrode/Li2S–P2S5 electrolyte prepared via mechanochemical reaction. *J. Power Sources* 189, 629–632. doi:10.1016/j.jpowsour.2008.09.064

Pan, H., Chen, J., Cao, R., Murugesan, V., Rajput, N. N., Han, K. S., et al. (2017). Non-encapsulation approach for high-performance Li–S batteries through controlled nucleation and growth. *Nat. Energy* 2, 813–820. doi:10.1038/s41560-017-0005-z

Phuc, N. H. H., Kazuhiro, H., Hiroyuki, M., and Atsunori, M. (2020a). High ionic conductivity of Li3−2M PS4 (M = Ca or Mg) at high temperature. *Solid State Ionics* 351, 115324. doi:10.1016/j.ssi.2020.115324

Phuc, N. H. H., Morikawa, K., Mitsuhiro, T., Muto, H., and Matsuda, A. (2017). Synthesis of plate-like Li3PS4 solid electrolyte via liquid-phase shaking for all-solid-state lithium batteries. *Ionics* 23, 2061–2067. doi:10.1007/s11581-017-2035-8

Phuc, N. H. H., Takaki, M., Kazuhiro, H., Hiroyuki, M., and Atsunori, M. (2020b). Dual effect of MgS addition on li2s ionic conductivity and all-solid-state Li–S cell performance. *SN Appl. Sci.* 2, 1803. doi:10.1007/s42452-020-03604-2

Phuc, N. H. H., Takaki, M., Muto, H., Reiko, M., Kazuhiro, H., and Matsuda, A. (2020c). Sulfur–carbon nano fiber composite solid electrolyte for all-solid-state Li–S batteries. *ACS Appl. Energy Mater.* 3, 1569–1573. doi:10.1021/acsaem.9b02062

Seino, Y., Ota, T., Takada, K., Hayashi, A., and Tatsumisago, M. (2014). A sulphide lithium super ion conductor is superior to liquid ion conductors for use in rechargeable batteries. *Energy Environ. Sci.* 7, 627–631. doi:10.1039/c3ee41655k

Spannenberger, S., Miß, V., Klotz, E., Kettner, J., Cronau, M., Ramanayagam, A., et al. (2019). Annealing-induced vacancy formation enables extraordinarily high Li+ ion conductivity in the amorphous electrolyte 0.33 LiI+0.67 Li3PS4. *Solid State Ionics* 341. doi:10.1016/j.ssi.2019.115040

Tan, D. H. S., Wu, E. A., Nguyen, H., Chen, Z., Marple, M. A. T., Doux, J.-M., et al. (2019). Elucidating reversible electrochemical redox of Li6PS5Cl solid electrolyte. *ACS Energy Lett* 4, 2418–2427. doi:10.1021/acsenergylett.9b01693

Tatsumisago, M., and Hayashi, A. (2012). Superionic glasses and glass–ceramics in the Li2S–P2S5 system for all-solid-state lithium secondary batteries. *Solid State Ionics* 225, 342–345. doi:10.1016/j.ssi.2012.03.013

Yang, Y., Zheng, G., and Cui, Y. (2013). Nanostructured sulfur cathodes. *Chem. Soc. Rev.* 42, 3018–3032. doi:10.1039/c2cs35256g

Yao, X., Liu, D., Wang, C., Long, P., Peng, G., Hu, Y. S., et al. (2016). High-energy all-solid-state lithium batteries with ultralong cycle life. *Nano Lett.* 16, 7148–7154. doi:10.1021/acs.nanolett.6b03448

Yun, J. H., Kim, J. H., Kim, D. K., and Lee, H. W. (2018). Suppressing polysulfide dissolution via cohesive forces by interwoven carbon nanofibers for high-areal-capacity lithium-sulfur batteries. *Nano Lett.* 18, 475–481. doi:10.1021/acs.nanolett.7b04425

Conflict of Interest: The authors declare that the research was conducted in the absence of any commercial or financial relationships that could be construed as a potential conflict of interest.